Generalized Multiport Reciprocity Analysis of Surface-to-Surface Transitions Between Multiple Printed Transmission Lines

Nirod K. Das, *Member, IEEE*

Abstract—**A new method of analysis of surface-to surface transitions between arbitrary combinations of multilayered printed transmission lines using a general multiport reciprocity formulation is presented. The scattering parameter at a given port of the transition is computed by directly relating it to simple reactions of the known eigenfields of the particular port on various induced strip currents or slot electric fields of other transmission lines. With simplifying practical assumptions in this general analysis, and by use of an efficient "singularity extraction technique," equivalent circuit models for particular cases are extracted with simple closed-form expressions for the equivalent circuit parameters. The multiport scattering matrix of the transition completely describes the coupling characteristics of the transition, and via standard network analysis can be conveniently used for design optimization of any port terminations and/or matching circuits. Detailed case studies of the general analysis include: 1) a single-layered microstrip line-to-slotline transition, 2) a microstrip-to-crossed covered microstrip transition, 3) a double microstrip line-to-slotline transition, and 4) a stripline-to-dual slotline transition.**

I. Introduction

SURFACE-TO-SURFACE transitions between printed transmission lines are useful for multilevel integrated circuits, and are particularly attractive for multilevel feed network architectures of multilayer phased arrays [1]–[4]. Characterization of crossover transitions between conducting strips is also of significant interest in modeling parasitic couplings between metal lines in high-speed digital integrated circuits [5], [6]. An equivalent circuit model for a microstrip–slotline transition [7] has long been used, and a dynamic analysis for the stub-tuned microstrip–slotline transition has also been published [8]. A quasi-static model for a perpendicular strip-crossover has been developed in [5], with rigorous solutions reported in [6] for only a uniform dielectric case, and in [9] for a two-layer stub-tuned geometry. For a multilayer phased array application [1]–[4], many other types of transitions between two or more different combinations of multilayer transmission lines will be useful. A general, rigorous, and computationally efficient analysis of such large class of transitions involving arbitrary orientations of multiple transmission lines is warranted for successful design and understanding.

Manuscript received April 27, 1992; revised November 25, 1992.

The author is with the Weber Research Institute/Department of Electrical Engineering, Polytechnic University, Farmingdale, NY 11735.

IEEE Log Number 9209345.

In this paper, we present a general, full-wave analysis of multiport, multiple transmission line transitions using a multiport reciprocity formulation [10], [11]. Using this formulation, the scattered signal at a given port of the transition is directly related via reciprocity to the reactions of the known eigenfields of the particular port on various induced strip-currents and slot electric fields. This results in a simple and efficient modeling of the coupling mechanism, as will be discussed. With practical approximations in the reciprocity analysis, and using a "singularity extraction technique" to compute the various coupling factors, equivalent circuits of the transition can be directly extracted with simple, sometimes closed-form, expressions for the equivalent circuit parameters. In contrast, a "brute-force" moment method analysis similar to [8], [9] is considered strictly numerical in nature, and so computationally inefficient, where similar extraction of an equivalent circuit with simple expressions for the equivalent circuit parameters will not be possible.

The analysis has been implemented in spectral domain, in terms of spectral integrals of various field and current transforms. A general configuration of substrate layers is accounted for by using the multilayer spectral-domain Green's functions [12]–[14], whereas any arbitrary choice of transmission lines of the transition is handled by substituting in the analysis for the necessary propagation constants, characteristic impedances, and eigenfields or eigencurrents of the individual transmission lines [12], [15]–[17]. The arbitrary combinations of transmission lines, as well as any arbitrary relative orientations between them, are properly accounted for in our analysis by using a general form of reciprocity relationship. The general analysis provides the complete scattering matrix of the multiport transition, using which port terminations (stubs, matching circuits, etc.) can be included. Selected case studies of the general analysis are presented. Useful circuit models are derived from the general theory, with simple expressions for their circuit parameters.

II. General Theory

Fig. 1 shows the general geometry of a proximity transition of multiple printed transmission lines. The eigensolutions for the individual port transmission lines are described by their characteristic impedances, Z_{ci}, propagation constants, k_{ei}, the strip current or slot electric field distributions, and the

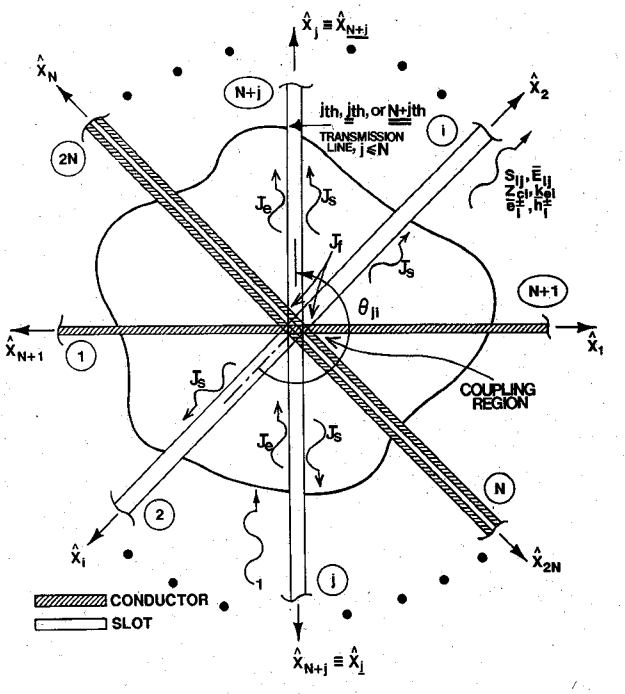

Fig. 1. General geometry of a transition with multiple planar transmission lines. The transmission lines (which can be a microstrip line, a slotline, a stripline, or a coplanar waveguide, for example) should be imagined to be printed on different layers of a multilayer substrate configuration. Different current components on the input, $\underline{j}$th, and a coupled, $\underline{i}$th, transmission line are shown.

eigenfields

$$\overline{E}_i^{\pm} = \overline{e}_i^{\pm} e^{\mp jk_{ei}x_i}; \qquad \overline{H}_i^{\pm} = \overline{h}_i^{\pm} e^{\mp jk_{ei}x_i}. \tag{1}$$

These eigensolutions are assumed to be known *a priori*. Full-wave printed transmission line analyses [12], [15]–[17] can be used in this effect. Further, the eigenfield distributions, $\overline{e}_i^{\pm}$ and $\overline{h}_i^{\pm}$, are assumed normalized to unit propagating power. Also, the transverse (to $\hat{x}_i$) components, $\overline{e}_{it}^{\pm}$ or $\overline{h}_{it}^{\pm}$, of the respective incoming (+) or outgoing (−) eigenfields of (1) are related to each other as

$$\overline{e}_{it}^{+} = \overline{e}_{it}^{-}, \qquad \overline{h}_{it}^{+} = -\overline{h}_{it}^{-}. \tag{2}$$

As Fig. 1 shows, a transition with N through transmission lines results in a $2N$ port circuit. For notational convenience, the two ports of the ith transmission line are assumed to be i and $N+i$, with $k_{ei} = k_{eN+i}$, $Z_{ci} = Z_{cN+i}$, and

$$\overline{e}_i^{\pm} = \overline{e}_{N+i}^{\mp}, \qquad \overline{h}_i^{\pm} = \overline{h}_{N+i}^{\mp}. \tag{3}$$

Further, for an arbitrary port, k, $k \le 2N$, the transmission line associated with the port is referred to as the $\underline{k}$th transmission line, and the port opposite to the kth port is referred to as the $\underline{k}$th port (see Fig. 1).

The $2N$ port transition of Fig. 1 is completely described by its $[2N \times 2N]$ scattering matrix $[S_{ij}]$. The scattering parameters can be characterized by exciting one port j at a time with unity incident power from a matched source, and computing the outgoing fields at all matched ports. Hence, in the following discussions, we would assume a single port (jth) excitation problem that can be repeated for all $1 \le j \le 2N$ to obtain the complete scattering matrix. Now, for this condition of jth port excitation, the strip electric currents or slot equivalent magnetic currents on the transmission lines $\overline{J}$ can be expressed as superposition of two different types of current modes, i.e., the traveling-wave part $\overline{J}_t$ of infinite or semiinfinite extent propagating toward or away from the junction region, and the additional nontraveling-wave currents of finite extent $\overline{J}_f$ in the vicinity of the transition. The traveling-wave currents $\overline{J}_t$ on the transmission lines can be further decomposed into (see Fig. 1) 1) the jth port excitation current $\overline{J}_e$ of infinite extent, and 2) the outgoing scattered currents $\overline{J}_{sk}$ of semiinfinite extent on kth transmission line, for all $k \le N$:

$$\overline{J} = \overline{J}_f + \overline{J}_t = \overline{J}_f + (\overline{J}_e + \overline{J}_s) = \overline{J}_f + \left[\overline{J}_e + \sum_{k=1}^{N} \overline{J}_{sk}\right], \tag{4}$$

$$\overline{J}_e = \overline{J}_{ej} = \overline{f}_j e^{-jk_{ej}x_j}; \qquad -\infty \le x_j \le \infty, \tag{5}$$

$$\begin{aligned}\overline{J}_{sk} &= [u(x_k)R_{k+N}\overline{f}_k e^{-jk_{ek}x_k} \\ &\quad + u(x_{k+N})R_k\overline{f}_{k+N}e^{-jk_{ek}x_{k+N}}] \\ &= R_{k+N}\overline{J}_{sk}^{f} + R_k\overline{J}_{sk}^{b}; \qquad k \le N,\end{aligned} \tag{6}$$

$$\begin{aligned}R_i &= S_{ij} - 1; \qquad i = \underline{j}, \\ &= S_{ij}; \qquad \text{otherwise},\end{aligned} \tag{7}$$

$$\begin{aligned}\overline{f}_k &= (f_{kx}(y_k)\hat{x}_k + f_{ky}(y_k)\hat{y}_k); \\ \overline{f}_{k+N} &= \pm(f_{kx}(y_{k+N})\hat{x}_{k+N} + f_{ky}(y_{k+N})\hat{y}_{k+N}),\end{aligned} \tag{8}$$

$$\begin{aligned}\overline{J}_f &= \sum_{k=1}^{N}\overline{J}_f^k = \sum_{k=1}^{N}\sum_{j=1}^{N_{fk}} I_{jk}\overline{J}_{fj}^k \\ &= \sum_{i=1}^{N_f} I_i\overline{J}_{fi}; \qquad N_f = \sum_{k=1}^{N} N_{fk},\end{aligned} \tag{9}$$

where $\overline{J}_f^k$ is the finite length current on the kth transmission line decomposed into N_{fk} modes, resulting in a total of N_f finite length modes of the system with unknown amplitudes I_i. $u(x)$ is the standard unit step function. $\overline{f}_k$ and $\overline{f}_{k+N}$ are the transverse variations of the forward and backward propagating semiinfinite traveling-wave currents, $\overline{J}_{sk}^{f}$ and $\overline{J}_{sk}^{b}$, respectively, with transverse Fourier transforms $\overline{F}_k(y_k)$ and $\overline{F}_{k+N}(y_{k+N})$. The $\overline{f}_k$ and $\overline{f}_{k+N}$ are chosen such that they correspond to the required unit propagating power for the kth transmission line eigenfield, as mentioned earlier. For example, for a single microstrip line, it requires the integral of f_{kx} over the strip width to be $1/\sqrt{Z_{ck}}$; whereas for a single slotline, it requires the integral of f_{kx} over the slot to be $\sqrt{Z_{ck}}$. Also, the $\pm$ sign before the expression for $\overline{f}_{k+N}$ in (8) is required to establish a common electric field reference for the two ports, k and $k+N$, at $x_k = x_{k+N} = 0$, and should be chosen to be positive (+) for a strip type kth transmission line, and negative (−) for a slot type kth transmission line with an equivalent magnetic current representation.

A. Reciprocity Formulation

Here we will use a general multiport reciprocity formulation in a similar basic form as that of [4], [14]. We will keep the basic formulational details to a minimum, emphasizing only the key steps that are exclusively new and vital to the transition modeling.

Now, the currents on all other transmission lines except the $\underline{i}$th transmission line can be treated as the sources of excitation $\overline{J}_S$ (or $\overline{M}_S$) for the outgoing scattered waves on th $\underline{i}$th transmission line of amplitudes R_i and $R_{\underline{i}}$ (see Fig. 2). These source currents, $\overline{J}_S$ (or $\overline{M}_S$)include all finite length currents, $\overline{J}_f^k$, $k \neq \underline{i}$; all scattered traveling-wave currents, $\overline{J}_{sk}$, $k \neq \underline{i}$; and the jth port excitation current, $\overline{J}_{ej}$, if $\underline{j} \neq \underline{i}$, as given by (4)–(9). One can now use a reciprocity treatment [10], [11], [4] to relate the scattered fields, R_i and $R_{\underline{i}}$, to the reaction of the incoming eigenfields of ports i and $\underline{i}$, respectively, on the excitation source $\overline{J}_S$. Consider the two sets of fields, identified with subscripts A and B, respectively, that are defined for the $\underline{i}$th transmission line at the ith and the $\underline{i}$th ports as (see Fig. 2):

$$\left.\begin{aligned} \overline{E}_A &= \overline{E}_{iA} = R_i \overline{E}_i^- \\ \overline{H}_A &= \overline{H}_{iA} = R_i \overline{H}_i^- \\ \overline{E}_B &= \overline{E}_{iB} = \overline{E}_i^+ \\ \overline{H}_B &= \overline{H}_{iB} = \overline{H}_i^+ \end{aligned}\right\}, \qquad \text{at } i\text{th port;}$$

$$\left.\begin{aligned} \overline{E}_A &= \overline{E}_{\underline{i}A} = R_{\underline{i}} \overline{E}_{\underline{i}}^- \\ \overline{H}_A &= \overline{H}_{\underline{i}A} = R_{\underline{i}} \overline{H}_{\underline{i}}^- \\ \overline{E}_B &= \overline{E}_{\underline{i}B} = \overline{E}_{\underline{i}}^- \\ \overline{H}_B &= \overline{H}_{\underline{i}B} = \overline{H}_{\underline{i}}^- \end{aligned}\right\}, \qquad \text{at } i\text{th port,} \tag{10}$$

with corresponding sources of excitation (surface currents)

$$\begin{aligned} &\overline{J}_{SA}\ (\text{or, } \overline{M}_{SA}) = \overline{J}_S\ (\text{or, } \overline{M}_S), \quad \text{and} \\ &\overline{J}_{SB}\ (\text{or, } \overline{M}_{SB}) = 0\,. \end{aligned} \tag{11}$$

Appropriately applying a reciprocity relation between the A and B fields [4], [10], [11], [14], and simplifying using (10), (11), (1), (2), we have (see Fig. 2)

$$\begin{aligned} &\iiint_{\text{sources}} \left(-\overline{E}_B \cdot \overline{J}_S + \overline{H}_B \cdot \overline{M}_S\right) dv = \\ &\qquad \oiint_S \left(\overline{E}_B \times \overline{H}_A - \overline{E}_A \times \overline{H}_B\right) ds \\ &\quad = \iint_{\text{port } i} \left(\overline{E}_B \times \overline{H}_A - \overline{E}_A \times \overline{H}_B\right) ds = 2R_i\,, \end{aligned} \tag{12}$$

$$R_i = \frac{1}{2} \iint_{\text{sources}} \left(-e^{-jk_{ei}x_i} \overline{e}_i^+ \cdot \overline{J}_S + e^{-jk_{ei}x_i} \overline{h}_i^+ \cdot \overline{M}_S\right) ds\,. \tag{13}$$

Similarly by choosing the B-fields in (10) to be propagating in the opposite direction, we will have

$$R_{\underline{i}} = \frac{1}{2} \iint_{\text{sources}} \left(-e^{jk_{ei}x_i} \overline{e}_{\underline{i}}^+ \cdot \overline{J}_S + e^{jk_{ei}x_i} \overline{h}_{\underline{i}}^+ \cdot \overline{M}_S\right) ds\,. \tag{14}$$

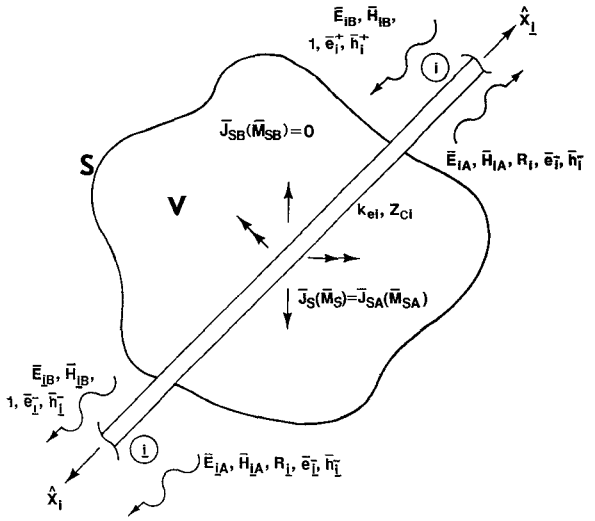

Fig. 2. Two sets of fields (subscripted A and B) on the $\underline{i}$th transmission line, with the corresponding sources, used for the reciprocity analysis. The closed surface S should be chosen sufficiently away from the coupling region such that the B-fields are zero at all other ports except the ith and $\underline{i}$th ports.

Further simplifying the reciprocity equations (13), (14) using the appropriate source expressions, $\overline{J}_S$(or $\overline{M}_S$), discussed earlier in this section

$$\begin{aligned} R_i = \frac{1}{2} \sum_{\substack{k=1 \\ k \neq \underline{i}}}^{N} \left(R_{k+N}\left(\pm V_{sik}^f\right) + R_k\left(\pm V_{sik}^b\right)\right) \\ + \frac{1}{2} \sum_{\substack{l=1 \\ l \text{ not on } \underline{i}}}^{N_f} I_l(\pm V_{fil}) + \frac{1}{2}\left(\pm V_{ei\underline{i}}\right), \qquad \underline{i} \neq \underline{j}, \end{aligned} \tag{15}$$

$$V_{ei\underline{j}} = \iint_{\underline{j}\text{th line}} e^{-jk_{ei}x_i} \overline{e}_i^+\left(\text{or, } \overline{h}_i^+\right) \cdot \overline{f}_{\underline{j}} e^{-jk_{e\underline{j}}x_{\underline{j}}}\, ds\,, \tag{16}$$

$$\begin{aligned} V_{sik}^f = \iint_{k\text{th line}} e^{-jk_{ei}x_i} \overline{e}_i^+\left(\text{or, } \overline{h}_i^+\right) \\ \cdot\ \overline{f}_k u(x_k) e^{-jk_{ek}x_k}\, ds\,, \end{aligned} \tag{17}$$

$$\begin{aligned} V_{sik}^b = \iint_{k\text{th line}} e^{-jk_{ei}x_i} \overline{e}_i^+\left(\text{or, } \overline{h}_i^+\right) \\ \cdot\ \overline{f}_{k+N} u(x_{k+N}) e^{-jk_{ek}x_{k+N}}\, ds\,, \end{aligned} \tag{18}$$

$$V_{fil} = \iint_{l\text{th mode}} e^{-jk_{ei}x_i} \overline{e}_i^+\left(\text{or, } \overline{h}_i^+\right) \cdot \overline{J}_{fl}\, ds\,, \tag{19}$$

where V's are the coupling integrals from the ith transmission line to different current modes on other transmission lines.

It should be noted, if the scattering source distribution, $\overline{f}$ or $\overline{J}_{fl}$, refer to an electric or an equivalent magnetic current mode, the eigenfields for the computation of V's in (16)–(19) must be chosen to be, eigen-electric $(\overline{e}_i^+)$, or eigen-magnetic

$(\overline{h}_i^+)$, respectively, and a $(+)$ or a $(-)$ sign, respectively, must be selected before the corresponding V's in (15). This is consistent with the general reciprocity equations (12)–(14). As before, in order to maintain generality, all current distributions, $\overline{f}$ or $\overline{J}_{fl}$ have been assumed to refer to either an electric or an equivalent magnetic current mode, as appropriate.

B. Moment Method Solution of Nontraveling-Wave Currents

In (15), we have directly established coupled relations among the different scattering parameters. If the currents on the transmission lines, including in the vicinity of the junction, are closely described by the infinite and semiinfinite traveling current modes alone (or $I_i = 0$), the reciprocity equation (15) will give a complete set of $2N$ equations to solve for the $2N$ unknown scattering parameters R_i. For some specific types of transitions, this is in fact the case, as discussed in Section III. In general, however, additional nontraveling-wave currents are induced in the vicinity of the junction, and are described by the finite mode currents, $\overline{J}_{fl}$, with unknown amplitudes, I_l, $l = 1, N_f$. To solve for these additional sets of N_f unknown amplitudes, a Galerkin's moment method procedure is used to provide the required N_f additional linear equations.

If the kth transmission line is a strip-type transmission line, the total tangential electric field, $\overline{E}_k^{tot}$, on its strips must be zero

$$\begin{aligned}\overline{E}_k^{tot} &= \overline{E}_{fk} + \overline{E}_{tk} = \overline{E}_{fk} + \overline{E}_{ek} + \overline{E}_{sk} = 0\\ &= \sum_{i=1}^{N_f} I_i \overline{E}_{fik} + \overline{E}_{ejk} + \sum_{i=1}^{N}\left(R_{i+N}\overline{E}^f_{sik} + R_i \overline{E}^b_{sik}\right)\end{aligned} \tag{20}$$

where the subscripts f, t, e and s refer to fields produced due to the scattering sources $\overline{J}_f$, $\overline{J}_t$, $\overline{J}_e$, and $\overline{J}_s$ of (4), respectively, with various indices corresponding to the respective source indices in (5), (6), (9). This zero tangential electric field boundary condition can be enforced variationally by a Galerkin's testing procedure on all finite current modes, $\overline{J}_{fl}$, $\tilde{l} = k$, on the kth transmission line

$$\sum_{i=1}^{N_f} I_i Z_{il} + v_{ejl} + \sum_{i=1}^{N}\left(R_{i+N} v^f_{sil} + R_i v^b_{sil}\right) = 0\,, \tag{21}$$

$$Z_{il} = \iint_{l\text{th mode}} \overline{E}_{fik}\cdot \overline{J}_{fl}\, ds\,, \tag{22}$$

$$\begin{aligned} v_{ejl} &= \iint_{l\text{th mode}} \overline{E}_{ejk}\cdot \overline{J}_{fl}\, ds\\ &= \iint_{l\text{th mode}} e^{-jk_{ej}x_j}\,\overline{e}_j^+ \cdot \overline{J}_{fl}\, ds;\\ &= 0, \qquad \text{if } j = \tilde{l}\,,\end{aligned} \tag{23}$$

$$v^{f,b}_{sil} = \iint_{l\text{th mode}} \overline{E}^{f,b}_{sik}\cdot \overline{J}_{fl}\, ds\,, \tag{24}$$

where the notation $\tilde{l}$, also to be used elsewhere, stands for the transmission line on which the lth finite mode, $\overline{J}_{fl}$, resides. Note that the reaction, v_{ejl} in (23), of the jth incident eigenfields on the lth finite mode is zero if $\tilde{l} = j$, which implies the eigenfields of a particular transmission line do not couple to the currents on itself.

On the other hand, if the kth transmission line is a slot type, the required boundary condition is the continuity of the tangential magnetic fields across its slots

$$\begin{aligned}\overline{H}_k^{tot1} - \overline{H}_k^{tot2} &= \left(\overline{H}^1_{fk} - \overline{H}^2_{fk}\right) + \left(\overline{H}^1_{tk} - \overline{H}^2_{tk}\right)\\ &= \left(\overline{H}^1_{fk} - \overline{H}^2_{fk}\right) + \left(\overline{H}^1_{ek} - \overline{H}^2_{ek}\right)\\ &\quad + \left(\overline{H}^1_{sk} - \overline{H}^2_{sk}\right) = 0\,.\end{aligned} \tag{25}$$

Enforcing this boundary condition via a Galerkin's testing procedure will result in a set of linear equations similar to (21), with

$$Z_{il} = Z^1_{il} + Z^2_{il} = \iint_{l\text{th mode}} \left(\overline{H}^1_{fik} - \overline{H}^2_{fik}\right)\cdot \overline{J}_{fl}\, ds\,, \tag{26}$$

$$\begin{aligned} v_{ejl} &= v^1_{ejl} + v^2_{ejl}\\ &= \iint_{l\text{th mode}} \left(\overline{H}^1_{ejk} - \overline{H}^2_{ejk}\right)\cdot \overline{J}_{fl}\, ds\\ &= \iint_{l\text{th mode}} e^{-jk_{ej}x_j}\left(\overline{h}_j^{+1} - \overline{h}_j^{+2}\right)\cdot \overline{J}_{fl}\, ds;\\ &= 0, \qquad \text{if } j = \tilde{l}\,,\end{aligned} \tag{27}$$

$$v^{f,b}_{sil} = v^{f1,b1}_{sil} + v^{f2,b2}_{sil} = \iint_{l\text{th mode}} \left(\overline{H}^{f1,b1}_{sik} - \overline{H}^{f2,b2}_{sik}\right)\cdot \overline{J}_{fl}\, ds\,, \tag{28}$$

where the superscripts 1 and 2 refer to field components above and below the slot, respectively.

To comprehend, Z_{il} is the reaction from the ith to the lth finite length basis modes, v^f_{sil} and v^b_{sil} are the reactions from, respectively, the forward $(\hat{x}_i)$ and backward $(\hat{x}_{i+N})$ propagating semiinfinite traveling currents on the ith transmission line to the lth finite mode, and v_{ejl} is the reaction from the jth infinite transmission line to the lth finite length mode.

C. Spectral-Domain Formulation

Now, the various reaction integrals (16)–(19), (22)–(24), and (26)–(28) can be implemented in spectral-domain using the multilayer full-wave Green's functions of [12]–[14] and Fourier transforms of current distributions

$$\begin{aligned} V_{eij} = \frac{1}{|\sin\theta_{ji}|}\overline{F}^*_j\left(k^i_{yj}\right)\cdot \overline{\overline{G}}\left(-k_{ei}, k^j_{yi}\right)\\ \cdot\ \overline{F}_i\left(k^j_{yi}\right) e^{jk_{ej}\Delta x_{ji}} e^{jk^i_{yj}\Delta y_{ji}}\,,\end{aligned} \tag{29}$$

$$V_{sik}^{f} = \frac{1}{2\pi}\int_{-\infty, k_{xi}=-k_{ei}}^{\infty} \overline{F}_k^*(k_{yk})\cdot\overline{\overline{G}}(-k_{ei}, k_{yi})\cdot\overline{F}_i(k_{yi})$$
$$H(-k_{xk}+k_{ek})e^{jk_{xk}\Delta x_{ki}}e^{jk_{yk}\Delta y_{ki}}\,dk_{yi}\,, \tag{30}$$

$$V_{sik}^{b} = \frac{1}{2\pi}\int_{k_{xi}=-k_{ei}}^{-\infty} \overline{F}_{k+N}^*(k_{yk+N})\cdot\overline{\overline{G}}(-k_{ei}, k_{yi})$$
$$\cdot\ \overline{F}_i(k_{yi})H(-k_{xk+N}+k_{ek+N})$$
$$e^{jk_{xk+N}\Delta x_{k+N_i}}e^{jk_{yk+N}\Delta y_{k+N_i}}\,dk_{yi}\,, \tag{31}$$

$$V_{fil} = \frac{1}{2\pi}\int_{-\infty, k_{xi}=-k_{ei}}^{\infty} \widetilde{\overline{J}}_{fl}^*(k_{xm}, k_{ym})\cdot\overline{\overline{G}}(-k_{ei}, k_{yi})$$
$$\cdot\ \overline{F}_i(k_{yi})\,dk_{yi};\qquad m=\tilde{l}\,, \tag{32}$$

$$Z_{il} = \frac{1}{4\pi^2}\iint_{-\infty}^{\infty} \widetilde{\overline{J}}_{fl}^*(k_{xm}, k_{ym})\cdot\overline{\overline{G}}(k_{xn}, k_{yn})$$
$$\cdot\ \widetilde{\overline{J}}_{fi}(k_{xn}, k_{yn})\,dk_{xn}\,dk_{yn};\qquad m=\tilde{l},\qquad n=\tilde{i}\,, \tag{33}$$

$$v_{sil}^{f} = \frac{1}{4\pi^2}\iint_{-\infty}^{\infty} \widetilde{\overline{J}}_{fl}^*(k_{xm}, k_{ym})\cdot\overline{\overline{G}}(k_{xi}, k_{yi})$$
$$\cdot\ \overline{F}_i(k_{yi})H(k_{xi}+k_{ei})\,dk_{xi}\,dk_{yi}\,, \tag{34}$$

$$v_{sil}^{b} = \frac{1}{4\pi^2}\iint_{-\infty}^{\infty} \widetilde{\overline{J}}_{fl}^*(k_{xm}, k_{ym})$$
$$\cdot\overline{\overline{G}}(k_{xi+N}, k_{yi+N})$$
$$\cdot\overline{F}_{i+N}(k_{yi+N})H(k_{xi+N}+k_{ei})$$
$$dk_{xi+N}\,dk_{yi+N}, \tag{35}$$

$$v_{ejl} = V_{fjl}\,, \tag{36}$$

$$k_{yi}^{j} = k_{ei}\cot\theta_{ji} + k_{ej}\csc\theta_{ji};$$
$$k_{yj}^{i} = k_{ei}\csc\theta_{ji} + k_{ej}\cot\theta_{ji}\,, \tag{37}$$

$$H(k_x) = \frac{-j}{k_x}\,. \tag{38}$$

In the above equations, the $\overline{\overline{G}}$'s are the full-wave dyadic Green's functions in spectral domain with appropriate source and field components and positions. $(\Delta x_{ji}, \Delta y_{ji})$ is the offset, if any, of the reference point of the jth transmission line with respect to that of the ith transmission line in the (x_j, y_j) coordinate system (see Fig. 1). As a common practice, the finite basis modes are assumed to be expressed with respect to the coordinate system of the associated $\tilde{l}$th transmission line. The test current transforms, $\overline{F}$ and $\widetilde{\overline{J}}$, are assumed to be expressed with respect to their own local coordinate systems (the test coordinate system (k_{xm}, k_{ym}) in (32), for example), but need to be changed to a common source coordinate system [(k_{xi}, k_{yi}) in (32), for example] before performing the necessary spectral-domain coupling integrals. If $\widetilde{\overline{J}}_{fl}(k_{xm}, k_{ym})$ is the transform of the lth finite length mode on the (k_{xm}, k_{ym}) plane ($\tilde{l}=m$), the new transform $\widetilde{\overline{J}}_{fl}^{t}(k_{xi}, k_{yi})$ on the (k_{xi}, k_{yi}) plane can be expressed

$$\widetilde{\overline{J}}_{fl}^{t}(k_{xi}, k_{yi}) = \widetilde{\overline{J}}_{fl}(k_{xm}^{t}, k_{ym}^{t})e^{-jk_{xm}^{t}\Delta x_{mi}}e^{-jk_{ym}^{t}\Delta y_{mi}}\,, \tag{39}$$

$$k_{ym}^{t} = -k_{xi}\sin\theta_{mi} + k_{yi}\cos\theta_{mi};$$
$$k_{xm}^{t} = k_{xi}\cos\theta_{mi} + k_{yi}\sin\theta_{mi}\,, \tag{40}$$

where as shown in Fig. 1, θ_{mi} is the angle between the mth and ith coordinate systems.

It should be noted that the spectral-domain coupling function, V_{eij}, is a closed-form expression not requiring an integration. This is because both the source and the coupled modes are infinite length transmission line modes. The coupling functions V_{sik}^{f}, V_{sik}^{b}, and V_{fil} are associated with an infinite length source mode but a noninfinite (finite or semiinfinite length) coupled mode, and so require simple single spectral integrals for evaluation. In contrast, for the other coupling functions Z_{il}, v_{sil}^{f}, and v_{sil}^{b}, both the source and coupled modes are of noninfinite type, and so they are expressed using two-dimensional spectral integrals. Because the reciprocity equations (15)–(19) involve only the simpler closed-form or single-dimensional integral functions V_{eij}, V_{sik}^{f}, V_{sik}^{b}, and V_{fil}, essential information on the coupling mechanism are thus efficiently extracted through the reciprocity modeling.

D. Singularity Extraction Technique

As discussed in [4], it is important to note that the Fourier transforms of the scattered currents J_{sk}, in (6), contain singularities at $\pm k_{ek}$ along the real k_{xk} spectral axis. In order to evaluate various spectral coupling integrals involving J_{sk}, it requires suitable deformation of the integration contour above and below the poles at $+k_{ek}$ and $-k_{ek}$, respectively, on the complex k_{xk} spectral plane [4]. Besides, the various spectral Green's functions that relate the appropriate field components to the source currents also have singularities on complex plane, as usual. Evaluating various spectral integrals, V and v in (29)–(36), involving the above singular functions require careful interpretation as well as special numerical and analytical considerations.

Consider the coupling integral V_{sik}^{f}, in (30), that needs to be evaluated along the required deformed contour C, as discussed above [4]. We decompose V_{sik}^{f} into two separate integrals, I_1 and I_2, as follows:

$$V_{sik}^{f} = \frac{1}{2\pi}\int_{-\infty, C}^{\infty}\gamma_1\,dk_{yi} = I_1 + I_2\,, \tag{41}$$

$$I_1 = \frac{1}{2\pi}\int_{-\infty, k_{xi}=-k_{ei}}^{\infty}[\overline{F}_k^*(k_{yk})\cdot\overline{\overline{G}}(-k_{ei}, k_{yi})\cdot\overline{F}_i(k_{yi})$$
$$H(-k_{xk}+k_{ek})e^{jk_{xk}\Delta x_{ki}}e^{jk_{yk}\Delta y_{ki}} - \gamma_2]\,dk_{yi}$$
$$= \frac{1}{2\pi}\int_{-\infty}^{\infty}(\gamma_1-\gamma_2)\,dk_{yi}\,, \tag{42}$$

$$I_2 = \overline{F}_k^*(k_{yk}^i) \cdot \bar{\bar{G}}(-k_{ei},\, k_{yi}^k) \cdot \overline{F}_i(k_{yi}^k)$$
$$e^{jk_{ek}\Delta x_{ki}} e^{jk_{yk}^i \Delta y_{ki}}$$
$$\frac{1}{2\pi}\int_{-\infty,\,C}^{\infty} H(k_{ek}-k_{xk})\,dk_{yi}$$
$$= \frac{1}{2\pi}\int_{-\infty}^{\infty} \gamma_2\,dk_{yi} = \frac{1}{2}\,V_{eik}\,, \tag{43}$$
$$\frac{1}{2\pi}\int_{-\infty,\,C}^{\infty} H(k_{ek}-k_{xk})\,dk_{yi} = \frac{1}{2|\sin\theta_{ki}|}\,, \tag{44}$$

where it can be shown that the integral I_1 is a well-behaved integral that can be efficiently computed along the real axis. On the other hand, the singularity of the integral, V_{sik}^f has been effectively extracted onto I_2. I_2 is a simple singular integral that has been analytically evaluated along the proper deformed contour, C. Fig. 3 shows the original, γ_1, and the extracted, $\gamma_1-\gamma_2$, integrands of V_{sik}^f, for the crossover coupling between two intersecting microstrip lines, along with the pole locii and the path of integration on the real $(k_{xi},\, k_{yi})$ plane. Fig. 3 clearly shows the original singular integral, and the well-behaved extracted integral. Note that the surface-wave poles due to the Green's functions are not encountered by the path of integration. This assumes that the individual transmission lines are desirably nonleaky type [17], with propagation constants greater than that of the surface modes.

Unlike the coupling integral, V_{sik}^f, discussed above, v_{sil}^f is a double integral over the entire $(k_{xi},\, k_{yi})$ space. Hence, in the domain of integration of v_{sil}^f, we will encounter not only the pole due to the semiinfinite traveling-wave transform, but also the pole due to the spectral Green's function. Extraction of multiple singularities of two-dimensional spectral coupling integrals using multiple extraction functions has been discussed in [4] and [14], and is not repeated here.

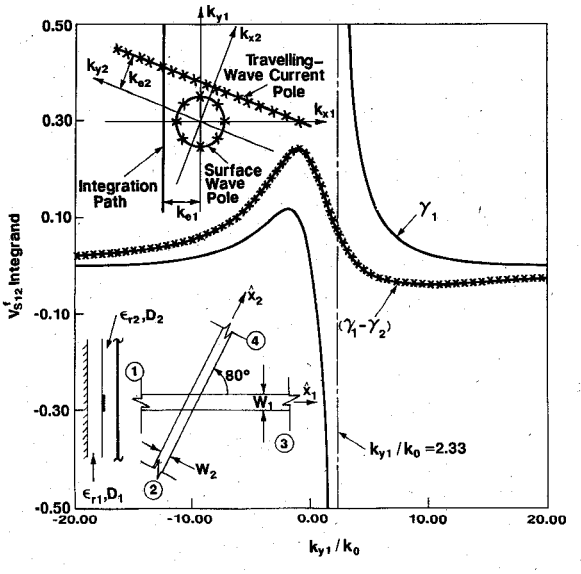

Fig. 3. Original (γ_1) and extracted $(\gamma_1-\gamma_2)$ integrands for the computation of coupling between the incident wave at port-1 and the forward scattered mode $(\overline{J}_{s2}^f)$ at port 2: $\epsilon_{r1}=2.2$, $\epsilon_{r2}=10.2$, $D_1=D_2=0.0635$ cm, $W_1=0.107$ cm, $W_2=0.183$ cm, $Z_{c1}\simeq 52\,\Omega$, $Z_{c2}\simeq 54\,\Omega$, $\epsilon_{eff1}\simeq 3.40$, $\epsilon_{eff2}\simeq 3.91$, freq. $=10$ GHz.

III. Results

We now apply the general analysis to selected transition geometries. Any stub and/or matching circuit of a practical transition geometry is accounted for via the multiport scattering matrix obtained from the general reciprocity analysis. Such a network approach is strictly valid only if the fields of the stub terminations do not directly interact with the fields in the vicinity of the transition. This condition is applicable to the stub-tuned geometries we have studied here, as well as many other practical transition configurations. In such cases, the end-corrections of the stubs, if critical, can be separately analyzed independent of the transition [18]–[20], and then incorporated as the port termination of the transition via the multiport scattering matrix. In other words, the transition coupling and the end-discontinuity of the tuning stubs are considered as two distinct problems electrically independent of each other. We have limited the scope of our paper to the rigorous modeling of the transition coupling alone. Unless otherwise mentioned, a stub has been assumed ideal without including any end-correction, which in most cases results in only second-order corrections. A colinear transition similar to [21], where the open ends of the transmission lines are essentially inseparable from the transition coupling, cannot be handled by the present analysis.

A. Microstrip-to-Slotline Transition

Fig. 4(a) shows the general geometry of a transition between a microstrip line and a slotline, which are generally inclined at an angle θ. Using the reciprocity/moment method analysis discussed in Section II, this transition can be rigorously analyzed to obtain the complete four-port scattering parameters. However, several degrees of practical approximations can be possible neglecting non-dominant coupling effects. We will specifically discuss such approximations for a perpendicular transition. The approximations have been validated by comparing to our most rigorous results and other results from literature.

Consider the transition geometry of Fig. 4(a), with $\theta = 90°$. We apply the general reciprocity analysis of Section II to this perpendicular transition, neglecting the finite length nontraveling-wave currents $\overline{J}_f$ in (4), (9). Assume the following transverse variations in (8):

$$\overline{f}_1 = \left(\frac{1}{\pi\sqrt{Z_{cm}}}\right)\frac{1}{\sqrt{(W_m/2)^2-y_1^2}}\,\hat{x}_1;$$
$$\overline{f}_2 = \left(\frac{\sqrt{Z_{cs}}}{\pi}\right)\frac{1}{\sqrt{(W_s/2)^2-y_2^2}}\,\hat{x}_2\,, \tag{45}$$

described over the strip-width of the microstrip line, or the slot-width of the slotline, respectively. For excitation at port 1, using proper symmetry considerations for coupling between different ports, the reciprocity equation (15) can be written

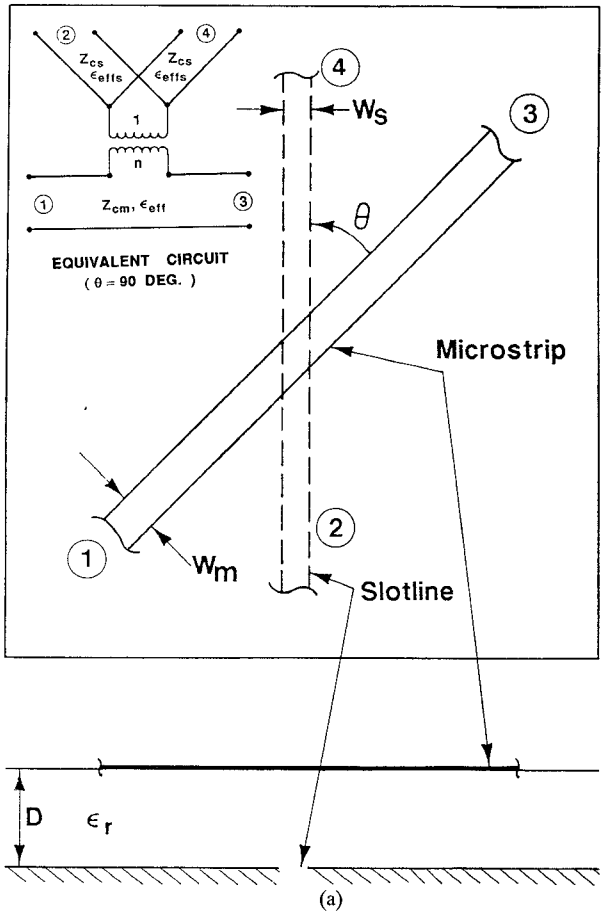

(a)

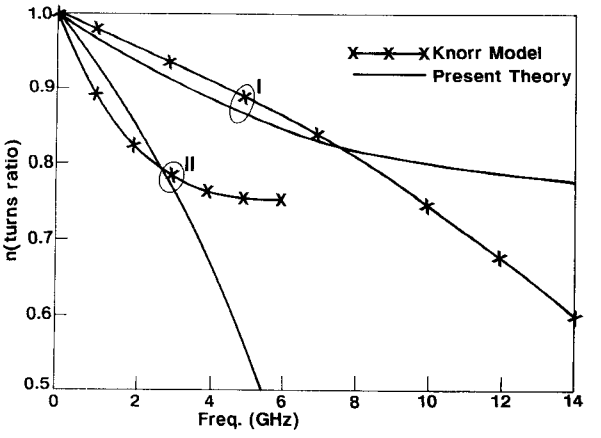

(b)

Fig. 4. (a) Geometry of a four-port transition between a microstrip line and a slotline, which are, in general, inclined with each other at an angle θ. The simplified equivalent circuit for the transition when $\theta = 90°$ is shown as the insert. (b) Comparison of equivalent turns ratio n for a perpendicular microstrip–slotline transition obtained from the present reciprocity model (49) with that of Knorr's model [7]: curve I—$D = 0.3175$ cm, $\epsilon_r = 20$, $W_m = 0.157$ cm, $W_s = 0.206$ cm, curve II—$D = 0.12$ cm, $\epsilon_r = 10.2$, $W_m = 0.12$ cm, $W_s = 0.11$ cm.

as

$$\begin{aligned} R_1 &= S_{11} = -R_3 = 1 - S_{31} = \frac{1}{2}\left(R_4 V_{s12}^f + R_2 V_{s12}^b\right) \\ &= S_{41} V_{s12}^f; \\ R_2 &= -\frac{1}{2} V_{e21} - \frac{1}{2}\left(R_3 V_{s21}^f + R_1 V_{s21}^b\right) \\ &= \frac{1}{2} V_{e12} - R_1 V_{s21}^b; \\ R_2 &= R_4 = S_{41} = S_{21}; \qquad V_{s12}^f = V_{s12}^b; \\ V_{s21}^f &= -V_{s21}^b; \qquad V_{e12} = -V_{e21}. \end{aligned} \tag{46}$$

These complete sets of equations can be solved for all S_{i1}. Similarly solving for excitation at other ports, by substituting appropriate V's in (46), we obtain the other scattering parameters, S_{ij}, $j = 2, 3, 4$. The required V's may be computed from (29)–(31), that involve only closed-form functions or single spectral integrals. With further simplification based on the singularity extraction derivations of (41)–(44), we obtain the following approximations:

$$\begin{aligned} V_{sik}^f \simeq \frac{1}{2} V_{eik} = -\frac{1}{2} V_{ek\underline{i}}; \\ V_{sik}^b \simeq \frac{1}{2} V_{ei\underline{k}} = -\frac{1}{2} V_{e\underline{k}i}; \\ i, k = 1, 2; \qquad i \neq k. \end{aligned} \tag{47}$$

The above approximations are valid if in (41)–(44) the contribution from the extracted integral I_1 is neglected as compared to the extraction function I_2. Physically, this implies that the coupling to a semiinfinite current mode is approximated by half the coupling to the respective infinite traveling-wave current, neglecting the additional reactive coupling to the discontinuity of the semiinfinite mode. Using these approximations of (47) in (46), we get

$$\begin{aligned} S_{11} &= 1 - S_{31} = \frac{1}{2} S_{41} V_{e12} = S_{33}; \\ S_{21} &= S_{41} = S_{23} = S_{43} = \frac{1}{2} V_{e12} - \frac{1}{2} S_{11} V_{e23} \\ &= \frac{1}{2} V_{e12}(1 - S_{11}); \\ V_{e12} &= V_{e14}; \qquad V_{e23} = -V_{e21} = V_{e12}; \\ S_{22} &= S_{24} - 1 = S_{44} = -\frac{1}{2} S_{12} V_{e23} = -\frac{1}{2} S_{12} V_{e12}; \\ S_{ij} &= S_{ji}. \end{aligned} \tag{48}$$

These above-mentioned sets of relations result in the equivalent circuit shown in Fig. 4(a) (insert), where the turns ratio n can be expressed as

$$\begin{aligned} n &= V_{e12}\sqrt{\frac{Z_{cm}}{Z_{cs}}} \\ &= J_0(k_{es}W_m/2)J_0(k_{em}W_s/2)\tilde{G}_{H_yJ_x}(-k_{em}, k_{es}) \\ &= \frac{J_0(k_{es}W_m/2)J_0(k_{em}W_s/2)}{k_{es}^2 + k_{em}^2} \\ &\quad \cdot \left[\frac{k_{em}^2 k_2 \epsilon_r}{(k_2\varepsilon_r \cos k_1 D - k_1 \sin k_1 D)} \right. \\ &\quad \left. + \frac{k_{es}^2 k_1}{(k_1 \cos k_1 D + k_2 \sin k_1 D)} \right], \end{aligned} \tag{49}$$

where V_{e12} is evaluated using (29); the Green's function component, $\tilde{G}_{H_yJ_x}$, accounts for the y-component of the magnetic field on the ground plane produced due to an x-directed current source placed on top of the substrate [12]–[14]; J_0 is the zeroth-order Bessel function; and

$$\begin{aligned} k_1 &= \sqrt{|k_0^2\epsilon_r - k_{es}^2 - k_{em}^2|} = k_0\sqrt{|\epsilon_r - \epsilon_{ffs} - \epsilon_{effm}|}\,; \\ k_2 &= k_0\sqrt{|\epsilon_{effs} + \epsilon_{effm} - 1|}\,; \\ k_{es} &= k_0\sqrt{\epsilon_{effs}}\,; \qquad k_{em} = k_0\sqrt{\epsilon_{effm}}\,. \end{aligned} \tag{50}$$

This expression for turns ratio n uses accurate distributions of microstrip current and slot electric field with proper edge singularity, as well as the exact spectral Green's function expressions. It realistically depends on the microstrip parameters (W_m, ϵ_{effm}), as well as the slotline parameters (W_s, ϵ_{effs}). In contrast, the ad hoc expression of Knorr [7] unrealistically depends on the slotline parameters alone. Our values of n are compared to those of [7] in Fig. 4(b) for two parameter sets. The two methods provide comparable results for lower frequencies, with unity at $dc\,(f \simeq 0)$, as expected. However, the two methods significantly deviate at higher frequencies suggesting the inaccuracy of the Knorr's model [7] for high-frequency applications. Moreover, our equation (49) provides a general closed-form expression that is also applicable to other microstrip–slotline transitions with multilayer substrate geometries. Such flexibility is achieved by substituting in (49) the proper values of propagation constants, k_{em} and k_{es}, for the multilayer microstrip line and slotline [12]–[15], [17], and the appropriate expression for the multilayer Green's function [12]–[14].

Fig. 5 compares various results for a perpendicular stub-tuned transition. The curve (a) has been derived using the equivalent circuit model of Fig. 4(a), where the turns ratio n is given by the closed-form expression of (49). The curve (b) uses the reciprocity equations (46), and unlike the curve (a) it does not use the approximations of (47). Clearly, both curves (a) and (b) neglect the finite length nontraveling-wave current modes in the vicinity of the junction, whereas curve (c) has been obtained using the most rigorous reciprocity formulation, including the additional finite length current modes $\overline{J}_f$ in (4), (9). It may be noted that our reciprocity analysis provides the 4-port scattering parameters, using the reflections from

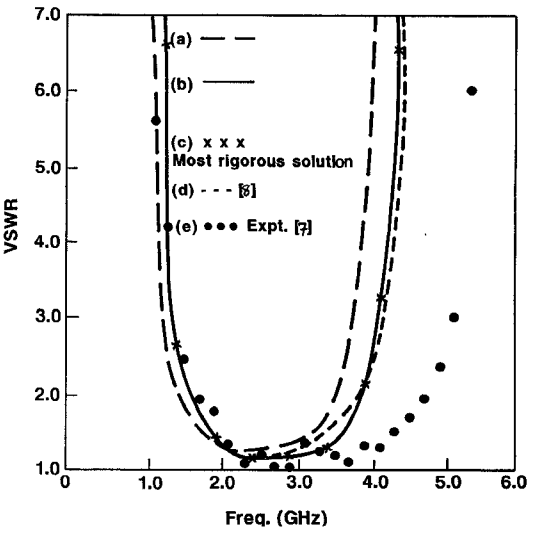

Fig. 5. Comparison of VSWR at the input microstrip port of a stub-tuned microstrip–slotline transition. Microstrip stub length = 0.688 cm, slotline stub length = 0.688 cm, both measured from the center of the transition. $\epsilon_r = 20$, $D = 0.3175$ cm, microstrip: $W_m = 0.157$ cm, $Z_{cm} \simeq 50\,\Omega$, $\epsilon_{effm} \simeq 13.78$, at 3.0 GHz.; slotline: $W_s = 0.206$ cm, $Z_{cs} \simeq 85\,\Omega$, $\epsilon_{effs} \simeq 8.3$, at 3.0 GHz.

the microstrip and slotline stubs which are included in order to obtain the two-port transition data of Fig. 5. The stub lengths are compensated for by the additional end effects using [19], [20]. Theoretical results of [8] [curve (d)], and measurement of [7] [curve (e)], are also presented in Fig. 5 for reference. Comparing curves (b) and (c), it is clear that the additional finite length current modes do not have significant effect on coupling. The equivalent circuit model of curve (a) provides reasonable results, but exhibits poorer bandwidth characteristics. Our rigorous results are comparable with the analysis of [8], but tend to deviate from the measurement of [7]. As indicated in [8], the measurement of [7] could have been inaccurate due to slotline termination mismatch, substrate loss, and other experimental errors.

An inclined transition, instead of the perpendicular case, will potentially provide additional design flexibility. However, similar approximations of the general reciprocity analysis discussed above for a perpendicular case, neglecting nontraveling wave, finite length current excitations in the vicinity of the coupling region, may not be adequate for the general inclined case. A simple circuit model, similar to that shown in Fig. 4(a), will not also be possible here, requiring the use of our most rigorous form of the reciprocity/moment method formulation for the general inclined case.

B. Crossover Transition Between Two Microstrip Lines

Fig. 6 shows the geometry of a crossover transition between a microstrip line and a covered microstrip line inclined at angle θ. We have used the general multiport reciprocity analysis of Section II to rigorously analyze the four-port transition of Fig. 6. In addition to the infinite and semiinfinite traveling-wave currents, five finite length PWS (piecewise sinusoid) modes were used to account for the extra nontraveling-wave current excitation in the vicinity of the transition. Note that,

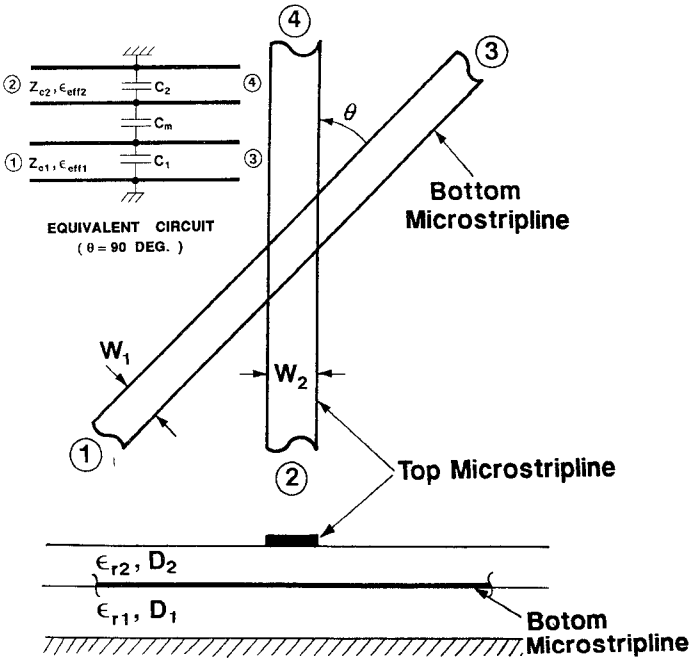

Fig. 6. Geometry of a four-port proximity (crossover) transition between a microstrip line and a covered microstrip line, inclined at an angle θ. The simplified equivalent circuit for the case of a perpendicular transition ($\theta = 90°$) using three coupling capacitors is shown as the insert.

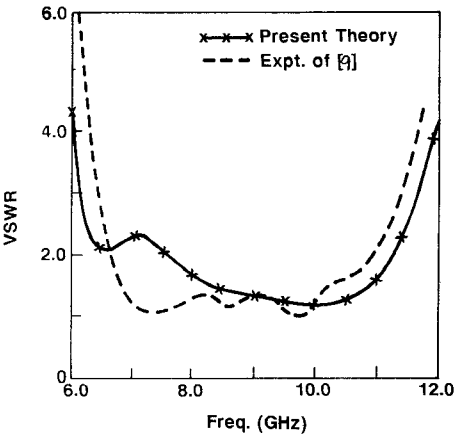

Fig. 7. VSWR at port 1 (see Fig. 6) of a stub-tuned microstrip-to-covered microstrip transition computed by the present method, as compared to the experiment of [9]: $W_{m1} = 0.107$ cm, $Z_{c1} \simeq 52\,\Omega$, $\epsilon_{eff1} \simeq 3.40$ (at 10 GHz.); $W_{m2} = 0.183$ cm, $Z_{c2} \simeq 54\,\Omega$, $\epsilon_{eff2} \simeq 3.91$ (at 10 GHz.); $\epsilon_{r1} = 2.2$, $D_1 = 0.0635$ cm, $\epsilon_{r2} = 10.2$, $D_1 = 0.0635$ cm; stub at port 3 = 0.81 cm, at port 4 = 0.75 cm.

unlike a perpendicular microstrip–slotline transition, the longitudinal components of the semiinfinite traveling-wave currents $\overline{J}_s$ on the microstrip lines of a crossover junction are not continuous across the reference plane, $x_i = 0$. This current discontinuity, on the microstrip line 1, for example, can be verified from (6), (8), where we have $R_1 \neq R_3$, and $\overline{f}_1 \cdot \hat{x}_1 = -\overline{f}_3 \cdot \hat{x}_1$. In order to ensure the required current continuity, additional half-PWS current modes have also been used in the rigorous analysis.

The complete 4-port scattering parameters obtained from the analysis are now used with stub terminations at ports 3 and 4 to model a two-port stub-tuned geometry. Fig. 7 shows the results for a two-port stub-tuned perpendicular transition, compared to the experimental results of [9]. The broadband nature of the transition is evident. Tight coupling between the two microstrip lines has been possible by using a higher dielectric constant substrate for the top layer resulting in more fringing fields from the bottom line coupling with the top line. Although the agreement of our results with the experiment of [9] in Fig. 7 has been good in terms of the general trend, coupling level and bandwidth, we cannot particularly explain the deviation of the results at the lower frequency end.

The modeling of unwanted parasitic capacitance between two crossover microstrip lines is of interest in high-speed digital integrated circuits. When the two microstrip lines are perpendicular to each other ($\theta = 90°$), the parasitic coupling for a perpendicular crossover can be quasi-statically modeled by three capacitors, as shown in Fig. 6. Such a simple model is, however, not valid for a general inclined transition. Also, although the coupling capacitance model will provide accurate results for digital integrated circuits, it will not be adequate for microwave frequencies. Using our reciprocity analysis with practical approximations, the equivalent coupling capacitances of Fig. 6 can be expressed in terms of simple closed-form expressions and single integrals. This provides an algorithm considerably faster than the existing methods [5], [6]. Also, the analysis of [6] is only applicable to a uniform dielectric medium, which certainly is not the case in practical integrated circuits. In contrast, our method is applicable to a general multilayered medium.

From the equivalent circuit of Fig. 6 for a perpendicular transition, it can be shown, in the limit of low frequency ($\omega \to 0$),

$$\left.\begin{aligned} S_{11} &\simeq \tfrac{-jw}{2}(C_m + C_1)Z_{c1} \\ S_{22} &\simeq \tfrac{-jw}{2}(C_m + C_2)Z_{c2} \\ S_{21} = S_{41} &\simeq \tfrac{jw}{2} C_m \sqrt{Z_{c1} Z_{c2}} \end{aligned}\right\}; \qquad \frac{1}{\omega C_{m,1,2}} >> Z_{c1,2}\,. \tag{51}$$

Let us use only the dominant longitudinal currents on the microstrip lines

$$\overline{f}_i = \left(\frac{1}{\pi\sqrt{Z_{ci}}}\right)\frac{1}{\sqrt{(W_i/2)^2 - y_i^2}}\,\hat{x}_i;$$
$$\overline{F}_i = \left(\frac{1}{\sqrt{Z_{ci}}}\right) J_0(k_{yi} W_i/2)\hat{x}_i; \qquad i = 1, 2\,. \tag{52}$$

In addition, neglect the finite length currents $\overline{J}_f$ in (4), (9). Under these assumptions, with excitation at port 1, the reciprocity equation (15) for a perpendicular transition can be written as

$$S_{11} = S_{31} - 1 = -\frac{1}{2}\left[S_{41}V_{s12}^f + S_{21}V_{s12}^b\right] = -S_{21}V_{s12}^f;$$
$$S_{21} = -\frac{1}{2}\left[V_{e21} + 2S_{11}V_{s21}^f\right];$$
$$S_{41} = S_{21}, \qquad V_{s12}^f = V_{s12}^b; \qquad V_{s21}^f = V_{s21}^b\,. \tag{53}$$

The different coupling parameters V can be computed from (29)–(31) using the appropriate Green's function components [12]–[14], and the current transforms of (52). Further, using the singularity extraction derivations of (42)–(44), we can show

$$V_{s12}^{f} = \frac{1}{2} V_{e12} + \Delta V_2 = -j \frac{\Delta V_1}{2} + \Delta V_2$$

$$V_{s21}^{f} = \frac{1}{2} V_{e21} + \Delta \acute{V}_2 = -j \frac{\Delta V_1}{2} + \Delta \acute{V}_2 , \qquad (54)$$

where ΔV_2 and $\Delta \acute{V}_2$ are the contributions from the respective extracted integrands, and $V_{e12} = V_{e21} = -j\Delta V_1$ is the coupling between the forward infinite traveling modes on the two lines that can be shown to be negatively imaginary. Unlike the perpendicular microstrip–slotline transition, here the singular contribution, $-j\Delta V_1$, is less significant than the extracted functions, ΔV_2 and $\Delta \acute{V}_2$. In the limit of $\omega \to 0$, we have $\Delta V_1 = 0$. This is due to the odd symmetry of the transverse electric field of one line that does not couple to a constant current on the other perpendicular line (as $\omega \to 0$, $e^{-jk_e x} \to$ a constant). On the other hand, ΔV_2 and $\Delta \acute{V}_2$ tend to a nonzero positive value as $\omega \to 0$. Now using (54) in (53), we get

$$S_{11} = -S_{21}\left(-j \frac{\Delta V_1}{2} + \Delta V_2\right)$$

$$S_{21} = j \frac{\Delta V_1}{2} - S_{11}\left(-j \frac{\Delta V_1}{2} + \Delta \acute{V}_2\right). \qquad (55)$$

S_{11} and S_{21} can now be solved from the above two equations. Using the quasi-static approximations discussed, where $\Delta V_1 << \Delta V_2, \Delta \acute{V}_2$

$$S_{11} = \frac{-j\Delta V_1 \Delta V_2}{2(1 - \Delta V_2 \Delta V_2)}$$

$$S_{21} = \frac{j\Delta V_1}{2\left(1 - \Delta V_2 \Delta \acute{V}_2\right)} . \qquad (56)$$

Comparing (56) to (51) we can write

$$C_m = \frac{\Delta V_1/\omega}{\left(1 - \Delta V_2 \Delta \acute{V}_2\right)} \frac{1}{\sqrt{Z_{c1} Z_{c2}}} , \qquad (57)$$

$$C_1 = \frac{\Delta V_1/\omega}{\left(1 - \Delta V_2 \Delta \acute{V}_2\right)} \left(\frac{\Delta V_2}{Z_{c1}} - \frac{1}{\sqrt{Z_{c1} Z_{c2}}} \right). \qquad (58)$$

Similarly, solving for the problem of excitation at port 2, by proper symmetry

$$C_2 = \frac{\Delta V_1/\omega}{\left(1 - \Delta V_2 \Delta \acute{V}_2\right)} \left(\frac{\Delta \acute{V}_2}{Z_{c2}} - \frac{1}{\sqrt{Z_{c1} Z_{c2}}} \right). \qquad (59)$$

The values of the coupling capacitances computed by the above simple formulas are compared in Fig. 8(a) to the results of [6] for a uniform dielectric case, showing good agreement. Such accuracy has also been obtained for practical crossover transitions with nonuniform or multiple substrates, as we verified by comparing to our rigorous results.

As mentioned before, the coupling capacitance model of Fig. 6 is not applicable for inclined transitions. The scattering

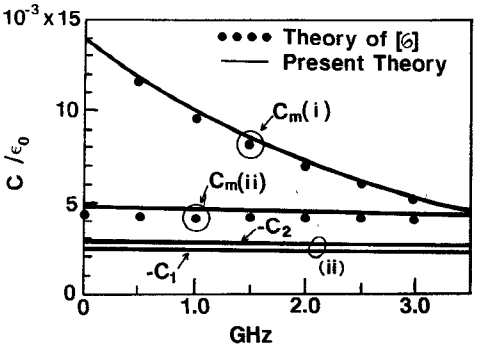

(a)

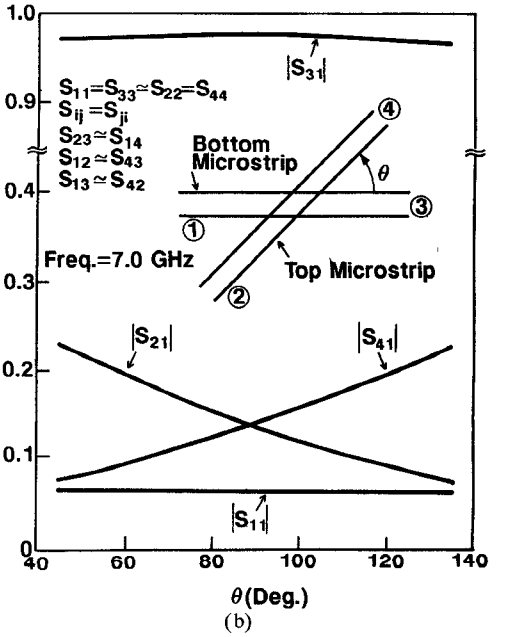

(b)

Fig. 8. (a) Comparison between the normalized coupling capacitance C_m for a perpendicular crossover transition, computed using the present reciprocity method, and the method of [6], for two sets of substrate thicknesses: (i) $D_1 = 1.0$ cm, $Z_{c1} \simeq 318\,\Omega$, $D_2 = 0.5$ cm, $Z_{c2} \simeq 342\,\Omega$; (ii) $D_1 = 0.1$ cm, $Z_{c1} \simeq 178\,\Omega$, $D_2 = 0.05$ cm, $Z_{c2} \simeq 203\,\Omega$; with $\epsilon_{r1} = 1.0$, $W_1 = 0.04$ cm, $\epsilon_{r2} = 1.0$, $W_2 = 0.04$ cm. The other equivalent capacitances, C_1 and C_2, are also shown for the case (ii). (b) The four-port scattering parameters of the above case (ii) with varying transition angle.

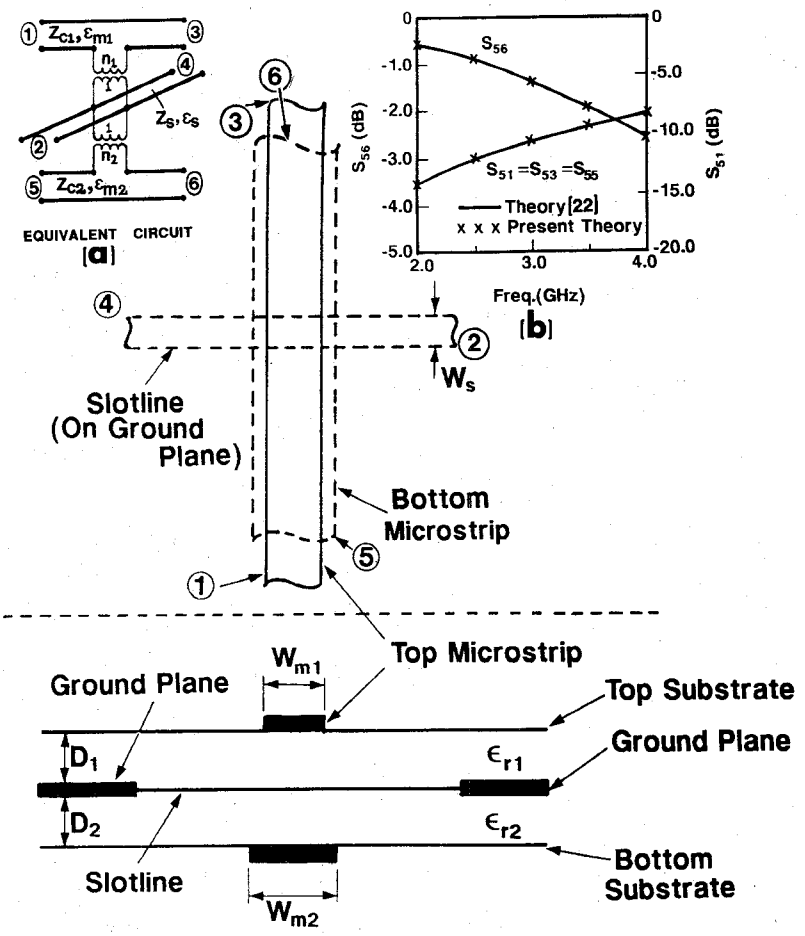

Fig. 9. Geometry of a six-port slotline-to-double microstrip transition, and (a) its equivalent circuit with different turns ratios for the two microstrip lines, (b) scattering parameters of a four-port stub-tuned geometry obtained by terminating the ports 2 and 4 with shorted slotline stubs. Results using our six-port analysis are compared to the results of [22]. Note that S_{51} and S_{55} are not, in general, the same, but are the same here due to the identical top and bottom microstrips. $\epsilon_{r1} = \epsilon_{r2} = 2.22$, $D_1 = D_2 = 0.0762$ cm, $W_{m1} = W_{m2} = 0.254$ cm, $W_s = 0.11$ cm, $L_{ss} = 0.75$ cm, slotline end correction = 0.3 cm.

matrix of an inclined crossover can, however, be obtained using our rigorous reciprocity analysis, that can be used to completely characterize the junction. Fig. 8(b) shows the scattering parameters for the transition of Fig. 8(a) as a function of the transition angle. The coupling to the ports 2 and 4 are weak, but exhibit a strong angular dependence. Also, the coupling to the port 2 can be significantly different from that to port 4, which clearly proves that the three-capacitance model of Fig. 6 is not valid here (the model of Fig. 6 would always result in the same coupling to port 2 and port 4).

C. Six-Port Double Microstrip-to-Slotline Transition

Fig. 9 shows the geometry of a six-port transition with a slotline coupled to two microstrip lines on both sides of its ground plane. A 3-port transition, coupling the input microstrip port 5 across its ground plane to the ports 1 and 3, can be designed by suitable tuning the ports 2, 4, and 6 by shorted or open stubs. In addition, one of the ports 1 or 3 can also be tuned by an open stub to realize a two-port transition across the ground plane from port 5 to port 3 or 1, respectively. The complete scattering parameters for the six-port geometry of Fig. 9 can be obtained from our general analysis, and used along with the necessary port terminations to characterize specific stub-tuned arrangements. Appropriate compensation for the stub end effects may be required for accurate results, however.

By terminating ports 2 and 4 with shorted slotline stubs of length L_{ss}, we have the four-port geometry of [22]. Results of our analysis are compared in Fig. 9(b) to the aperture analysis of [22], showing good agreement. It should be noted, in contrast to our method that the aperture-coupling analysis of [22] treats the slotline terminations at ports 2 and 4 as a finite "aperture," not as "two slotline stubs." The present multiport analysis is considerably simpler than that of [22]. The six-port scattering matrix, once evaluated using our analysis, can be used later to treat any slot lengths, or other stub arrangements. On the contrary, repeated analysis of [22] needs to be performed every time the slot length is changed for a design.

A simple equivalent circuit model, providing comparable results to the rigorous analysis will also be useful. Extending the equivalent circuit of Fig. 4(a), by including the additional coupling to a second microstrip line, in Fig. 9 we have shown a six-port equivalent circuit for the slotline-to-dual microstrip transition. Z_s and ϵ_s of the equivalent circuit are, respectively,

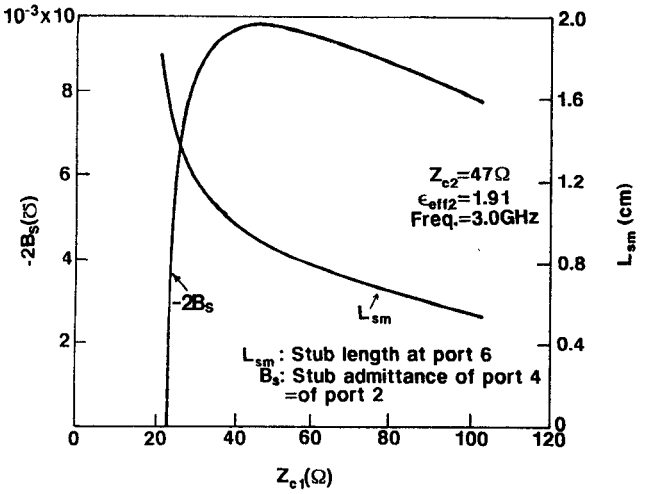

Fig. 10. Required combinations of slot-stub admittance B_s at ports 2 and 4, and the open microstrip stub length L_{sm} at port 6, for different values of characteristic impedances Z_{c1} of the top microstrip, in order to obtain a perfect input match at port 5.

the characteristic impedance and effective dielectric constant of a slotline with two substrates on the two sides of the ground plane, and can be determined using a full-wave general analysis of [16], [12], [17]. Also, the two microstrip lines above and below the slotline are in general different, and couple differently to the slotline in between. This has been accounted for by using two different turns ratios, n_1 and n_2, in the equivalent circuit of Fig. 9. Equation (49) can also be used here to compute n_1 as well as n_2 by substituting for the substrate and microstrip parameter of the respective sides.

The simple equivalent circuit model of Fig. 9 with closed-form expressions for the turns ratios can be particularly useful for initial design optimization and understanding when the rigorous analysis may be extremely time consuming or sometimes impractical to use. Consider a three-port geometry [22], where the port 5 of Fig. 9 is coupled to ports 1 and 3, with other three ports stub-tuned. Using the equivalent circuit of Fig. 9, it can be shown [23] that for a given input port impedance, Z_{c2}, different values of Z_{c1} would require unique combinations of the total slot-stub admittance, $2B_s$ (B_s for each stub at ports 2 and 4) at ports 2 and 4, and the open microstrip stub length, L_{sm}, at port 6, in order to obtain a perfect input match. These data are presented in Fig. 10 for $Z_{c2} \simeq 50\,\Omega$. It is interesting to note that it is not possible to get a perfect input match by tuning ports 2, 4, and 6, if Z_{c1} is less than about $25\,\Omega$. At this limiting value of Z_{c1}, the required $B_s = 0$ (a quarter-wavelength stub) and $L_{sm} \simeq 1.81$ cm. Also, a given value of B_s can be obtained using different combinations of slot width W_s (which determines Z_s and ϵ_s), and slot-stub length L_{ss} related as: $B_s Z_s = -\cot\left(k_0\sqrt{\epsilon_s}\,L_{ss}\right)$. Unwanted radiation loss from the short-circuited slotline section (strong radiation if the total slot length is close to a half-guide wavelength), and the bandwidth of the transition, are critical considerations in choosing the slot and microstrip stub dimensions.

D. Stripline-to-Dual Slotline Transition

A stripline-to-dual slotline transition is similar to a microstrip-to-slotline transition, where the microstrip line is replaced by a stripline and the regular slotline is replaced by a pair of identical slotlines (a dual slotline) printed on top and bottom groundplanes of the stripline. The two slotlines cut across the ground currents of the stripline flowing along the same directions. This excites identical electric fields across the two slots of the dual slotline. Such a dual slotline with an even-mode field excitation, unlike an odd-mode excitation case, does not experience any unwanted leakage to the parallel plate mode [17], [24], and has been successfully used in feeding dual tapered-slot antennas [25]. Fig. 11(a) shows the geometry of two stripline-to-dual slotline junctions, with their 4th ports cascaded, and 2nd and 3rd ports tuned using approximately quarter-wavelength open and shorted stubs, respectively. This cascaded geometry is suitable for characterization of the stripline-to-dual slotline transition, avoiding the need for a direct port connection with the dual slotline. The return loss measurement of [25] at the stripline input port 1, as compared to our rigorous analysis, is presented in Fig. 11(b). As before, the complete scattering matrix for a four-port transition is directly obtained from our general analysis, which is then used in duplicate accounting for throughline length L_{TH} and the various stub lengths, L_{SL} and L_{ST}. The impedance and propagation characteristics of the stripline and the dual slotline, necessary for the transition analysis and stub calculations, are obtained using the full-wave analysis of [12], [15]–[17]. The comparison of return-loss results in Fig. 11(b) is good, and demonstrates the accuracy and validity of our analysis. The possible excitation of the parallel plate mode at various discontinuities, and the related resonance effects [17], are the potential problems in practical designs. Shorting of the bottom and top ground planes may be desirable to avoid the excitations of any such unwanted parallel plate modes.

A simplified equivalent circuit similar to that of Fig. 4(a) is also applicable for a stripline-to-dual slotline transition, by appropriately substituting in Fig. 4(a) for the transmission line parameters and the turns ratio. The resulting equivalent circuit for the cascaded geometry of Fig. 11(a) is also shown. The turns ratio n for the geometry of Fig. 11(a) can be calculated from (49), where we need to use the appropriate Green's function for the present geometry [12], [13], and substitute for the microstrip and slotline parameters by those of the stripline and dual slotline, respectively. Referring to Fig. 11(a) for various parameters, we have

$$n = \frac{J_0\left(k_0\sqrt{\epsilon_{eff}}\,W_{ST}/2\right) J_0\left(k_0\sqrt{\epsilon_r}\,W_{SL}/2\right)}{2\cosh\left(k_0\sqrt{\epsilon_{eff}}\,d/2\right)}, \qquad (60)$$

where k_0 is the free space wave number. As frequency goes to zero ($k_0 \to 0$), we have $n \to 1$, as expected for the dc case. Results obtained using the equivalent circuit of Fig. 11(a), with the turns ratio expression of (60), are also compared in Fig. 11(b). As the comparison indicates, the equivalent circuit model for a stripline–dual slotline transition with simple closed-form expressions for its parameters can be effectively used to get fairly accurate results.

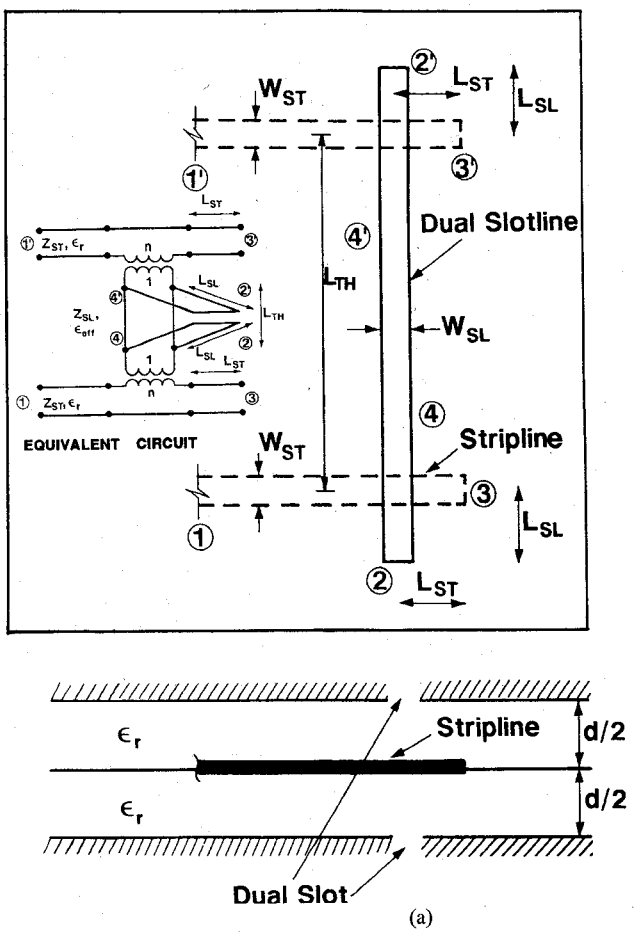

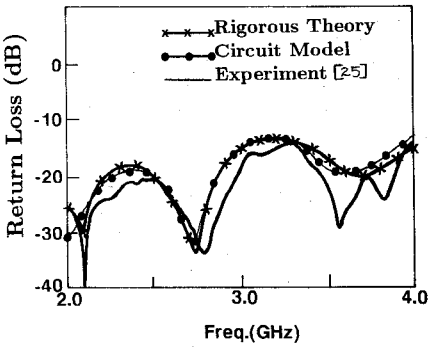

Fig. 11. (a) Two identical stub-tuned stripline-to-dual slotline junctions connected back to back, resulting in a stripline–dual slotline–stripline transition. Its equivalent circuit using coupling transformers and transmission line stubs is also shown. (b) Comparison of theoretical and experimental results of input return loss for the two-port stripline–dual slotline–stripline transition of (a). $\epsilon_r = 2.33$, $d = 0.1524$ cm, $W_{ST} = 0.125$ cm, $W_{SL} = 0.0254$ cm, $L_{ST} = 1.64$ cm, $L_{SL} = 2.2$ cm, $L_{TH} = 10.0$ cm.

REFERENCES

[1] R. J. Mailloux, "Phased array architectures for millimeter wave active arrays,"*IEEE Antennas Propagat. Soc. Newslett.,* vol. AP-28, pp. 5–7, Feb. 1986.

[2] N. K. Das and D. M. Pozar, "Printed antennas in multiple layers: General considerations and infinite array analysis using a unified method," in *Proc. IEEE Int. Conf. Antennas Propagat., ICAP,* Univ. Warwick, UK, Apr. 1989, pp. 364–368.

[3] J. A. Kinzel, "GaAs technology for millimeter wave phased arrays," *IEEE Antennas Propagat. Soc. Newslett.,* vol. AP-29, pp. 12–14, Feb. 1987.

[4] N. K. Das and D. M. Pozar, "Multiport scattering analysis of multilayered printed antennas fed by multiple feed ports, Part I: Theory; Part II: Applications," *IEEE Trans. Antennas Propagat.,* vol. AP-40, pp. 469–491, May 1992.

[5] S. Papatheodorou, R. F. Harrington, and J. R. Mautz, "The equivalent circuit of a microstrip crossover in a dielectric substrate," *IEEE Trans. Microwave Theory Tech.,* vol. MTT-38, pp. 135–140, Feb. 1990.

[6] ——, "Full-wave analysis of a strip crossover," *IEEE Trans. Microwave Theory Tech.* vol. MTT-38, pp. 1439–1448, Oct. 1990.

[7] J. B. Knorr, "Slot-line transitions," *IEEE Trans. Microwave Theory Tech.,* vol. MTT-22, pp. 548–554, May 1974.

[8] H. Yang and N. G. Alexopoulos, "A dynamic model for microstrip-slotline transition and related structures," *IEEE Trans. Microwave Theory Tech.,* vol. MTT-36, pp. 286–293, Feb. 1988.

[9] ——, "Basic blocks for high frequency Interconnects: Theory and experiment," *IEEE Trans. Microwave Theory Tech.,* vol. MTT-36, pp. 1258–1264, Aug. 1988.

[10] R. F. Harrington, *Time Harmonic Electromagnetic Fields.* New York: McGraw-Hill, 1984.

[11] D. M. Pozar, "A reciprocity method of analysis of printed slots and slot-coupled microstrip antennas," *IEEE Trans. Antennas Propagat.,* vol. AP-34, pp. 1439–1446, Dec. 1986.

[12] N. K. Das and D. M. Pozar, "A generalized spectral-domain Green's function for multilayer dielectric substrates with applications to multilayer transmission lines," *IEEE Trans. Microwave Theory Tech.,* vol. MTT-35, pp. 326–335, Mar. 1987.

[13] N. K. Das, "A study of multilayered printed antenna structures," Ph.D. dissertation, Dep. Elec. Comput. Eng., Univ. Mass., Amherst, Sept. 1987.

[14] N. K. Das and D. M. Pozar, "A generalized CAD model for printed antennas and arrays with arbitrary multilayer geometries," in *Computer Physics Communication, Thematic Issue on Computational Electromagnetics,* L. Safai, Ed. Amsterdam, The Netherlands: North Holland, 1991.

[15] ——, PCAAMT—*Personal Computer Aided Analysis of Multilayer Transmission Lines—Version 1.0,* Antenna Design Associates, Leverette, MA.

[16] ——, "Perform full-wave multilayer analysis on a PC," *Microwaves & RF Mag.,* pp. 125–132, Feb. 1992.

[17] ——, "Full wave spectral-domain computation of material, radiation and guided wave losses in infinite multilayered printed transmission lines," *IEEE Trans. Microwave Theory Tech.,* vol. MTT-39, pp. 54–63, Jan. 1991.

[18] R. W. Jackson and D. M. Pozar, "Full-wave analysis of microstrip open end and gap discontinuities," *IEEE Trans. Microwave Theory Tech.,* vol. MTT-33, pp. 1036–1042, Oct. 1985.

[19] P. Silvester and P. Benedek, "Equivalent capacitances of microstrip open circuits," *IEEE Trans. Microwave Theory and Tech.*, vol. MTT-20, pp. 511–516, Aug. 1972.
[20] J. B. Knorr and J. Saenz, "End effects in a shorted slot, *IEEE Trans. Microwave Theory Tech.*, vol. MTT-21, pp. 579–580, Sept. 1973.
[21] R. W. Jackson and D. W. Matolak, "Surface-to surface transition via electromagnetic coupling of coplanar waveguides," *IEEE Trans. Microwave Theory Tech.*, vol. MTT-35, pp. 1027–1032, Nov. 1987.
[22] N. Herscovici and D. M. Pozar, "Full-wave analysis of aperture-coupled microstrip lines," *IEEE Trans. Microwave Theory Tech.*, vol. MTT-39, pp. 1108–1114, July 1991.
[23] D. M. Pozar, *Microwave Engineering.* Reading, MA: Addison-Wesley, 1990.
[24] N. K. Das, "Characteristics of modified slotline configurations," in *IEEE Microwave Theory Tech. Symp. Dig.*, 1991, pp. 777–780.
[25] D. H. Schaubert, "Endfire slotline antennas," in *J. Int. Nice Antennes—JINA '90,* 1990, pp. 253–265.

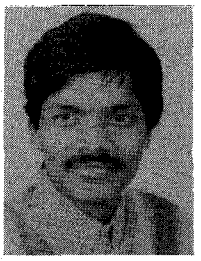

Nirod K. Das was born in Puri, Orissa State, India, on February 27, 1963. He received the B.Tech. (hons.) degree in electronics and electrical communication engineering from the Indian Institute of Technology (IIT), Kharagpur, India, in 1985, and M.S. and Ph.D. degrees in electrical engineering from the University of Massachusetts, Amherst, in 1987 and 1989, respectively.

From 1985 to 1989 he was with the Department of Electrical and Computer Engineering at the University of Massachusetts, Amherst, first as a Graduate Research Assistant and then, after receiving the Ph.D. degree, as a Postdoctoral Research Associate. In 1990 he joined the Department of Electrical Engineering, Polytechnic University, Farmingdale, NY, as an Assistant Professor. His research interests have been in the general areas of microwaves, millimeter waves, and optoelectronic integrated circuits and antennas, and, in particular, the analytical and experimental study of multiple-layered structures for integrated circuits and phased array applications.

Dr. Das has received a student prize paper award from USNC URSI during his doctoral studies, and received the 1992 RWP King Best Paper Award from IEEE Antennas and Propagation Society for his multilayer antenna work.